© 1996 Nature Publishing Group http://www.nature.com/naturegenetics

Glucose-6-phosphatase dependent substrate transport in the glycogen storage disease type-1a mouse

Ke-Jian Lei[1], Hungwen Chen[1], Chi-Jiunn Pan[1], Jerrold M. Ward[3], Bedrich Mosinger, Jr.[2,4], Eric J. Lee[2], Heiner Westphal[2], Brian C. Mansfield[1] & Janice Yang Chou[1]

Glycogen storage disease type 1a (GSD-1a) is caused by a deficiency in microsomal glucose-6-phosphatase (G6Pase), the key enzyme in glucose homeostasis. A *G6Pase* knockout mouse which mimics the pathophysiology of human GSD-1a patients was created to understand the pathogenesis of this disorder, to delineate the mechanisms of G6Pase catalysis, and to develop future therapeutic approaches. By examining G6Pase in the liver and kidney, the primary gluconeogenic tissues, we demonstrate that glucose-6-P transport and hydrolysis are performed by separate proteins which are tightly coupled. We propose a modified translocase catalytic unit model for G6Pase catalysis.

[1]*Heritable Disorders Branch and* [2]*Laboratory of Mammalian Genes and Development, National Institute of Child Health and Human Development, National Institutes of Health, Bethesda, Maryland 20892, USA*
[2]*Veterinary and Tumor Pathology Section, Office of Laboratory Animal Science, National Cancer Institute, Frederick, Maryland 21702, USA*
[4]*Current address: Laboratory of Molecular Genetics, Institute for Mother and Child Care, Prague, Czech Republic*

K.-J.L., H.C. and C.-J.P. contributed equally to the manuscript

Correspondence should be addressed to J.Y.C.

Glucose-6-phosphatase (G6Pase), the key enzyme in glucose homeostasis, is tightly associated with the endoplasmic reticulum (ER) and nuclear membranes of the liver and kidney[1]. In humans, deficiency of G6Pase activity causes glycogen storage disease type 1 (GSD-1) also known as von Gierke disease[2,3]. This autosomal recessive disorder is characterized by severe hypoglycaemia, growth retardation, hepatomegaly, kidney enlargement, hyperlipidaemia, hyperuricaemia, and lactic acidaemia[2,3]. Since the G6Pase active center is not exposed to the cytoplasm[4], G6Pase catalysis requires glucose-6-P (G6P) transport from the cytoplasm across the ER membranes before hydrolysis can occur. Currently, there are two models proposed for G6Pase catalysis. The conformation-substrate-transport model proposes that G6Pase is a multi-functional enzyme possessing catalytic and substrate/product transport activities[5]. This model is supported by observations that G6P transport and hydrolytic activities appear synchronous, suggesting that the two processes are tightly linked[6]. On the other hand, the translocase-catalytic unit model proposes that G6Pase is a multi-component system consisting of a catalytic unit and associated translocases[7]. This model has been used to explain the phenotypic divergence observed in the four GSD-1 subgroups, 1a, 1b, 1c and 1d, which correspond to defects in the G6Pase catalytic unit (1a), the putative G6P translocase (1b), the putative phosphate/pyrophosphate translocase (1c), and the putative glucose translocase (1d)[8]. The translocase-catalytic unit concept is also supported by kinetic and transport studies using liver specimens from GSD-1b and 1c patients whose liver microsomes lack G6P and pyrophosphate/phosphate transport activities, respectively, yet, when disrupted with detergent, contain high G6Pase enzymatic activity[9–12].

To gain insight into the mechanisms of G6Pase catalysis and the pathogenesis of GSD-1a, we have characterized the *G6Pase* cDNAs and genes[13,14]. These studies revealed that mammalian G6Pases are hydrophobic proteins containing six putative membrane-spanning segments. We have also identified a large number of disease-causing mutations in the *G6Pase* gene of GSD-1a patients[14,15], thus establishing the molecular basis of the GSD-1a disorder. However, we have not detected mutations in the *G6Pase* gene of GSD-1b and 1c patients[16], suggesting that, indeed, these patients may be defective in the putative translocases. Using a rodent model for GSD-1a we show a tight coupling between transport and catalysis, with an absolute requirement of G6Pase activity for G6P transport. Our results also show that liver and kidney have different G6P transport/hydrolytic activities, further supporting the involvement of more than one protein in G6P transport and G6P catalysis. We propose a modified translocase-catalytic-unit concept to explain the mode of G6Pase catalysis.

Generation of *G6Pase*-deficient mice

The *G6Pase* gene from the 129Sv/J mouse, spanning approximately 12 kb and containing all five exons was isolated, mapped, and partially sequenced (Fig. 1*a*). To disrupt the *G6Pase* gene, a targeting vector was constructed (Fig. 1*a*) in which exon 3 and the associated introns of the murine *G6Pase* gene were replaced with a neomycin (neo) cassette[17]. The 115-residue truncat-

© 1996 Nature Publishing Group http://www.nature.com/naturegenetics

ed G6Pase protein is expected to be enzymatically inactive[13,14]. A herpes simplex virus thymidine kinase (HSV-tk) cassette was also included in the construct for negative selection[17]. The construct was introduced into J1 ES cells[18] and the cells were subjected to selection with the drugs G418 and gancyclovir[19]. Southern blots of *Kpn*I and *Sfu*I digested genomic DNA were hybridized with 5'-flanking (probe A) and 3'-flanking (probe B) probes (Fig. 1*a*) to identify five targeted clones from 198 doubly resistant clones (Fig. 1*b*).

Cells from targeted ES cell clones were injected into blastocysts from C57BL/6 mice and transferred into FVB/N foster mothers. Two independent ES clones were used and germline transmission was achieved for each clone. Mice heterozygous for the disrupted *G6Pase* gene were mated, and homozygous mutant progenies were identified by PCR (Fig. 1*c*) and Southern blot (Fig. 1*d*) analysis of tail genomic DNAs.

A riboprobe that spans nucleotides 356 to 640 of the murine *G6Pase* cDNA[13], including the entire exon 3, detected a fully protected band of 285 bp in RNAs from liver and kidney of G6Pase$^{+/+}$ and G6Pase$^{+/-}$ mice (Fig. 1*e*). No signals were detected in G6Pase$^{-/-}$ mice, indicating the absence of the wild-type *G6Pase* mRNA. Western blot analysis confirmed that the G6Pase protein was present in the livers and kidneys of G6Pase$^{+/+}$ and G6Pase$^{+/-}$ mice but absent in homozygous G6Pase$^{-/-}$ mice (Fig. 1*f*). Moreover, significant G6Pase enzyme activity was detected in liver and kidney microsomes of G6Pase$^{+/+}$ mice while approximately 50% less was detected in G6Pase$^{+/-}$ mice (Fig. 1*g*). In the G6Pase$^{-/-}$ mouse tissues, there were no detectable G6Pase activities. The results confirmed that the targeted mutation in exon 3 had resulted in a null *G6Pase* locus *in vivo*.

Phenotype of the *G6Pase*-deficient mice

The GSD-1a disorder is not an embryonic lethal muta-

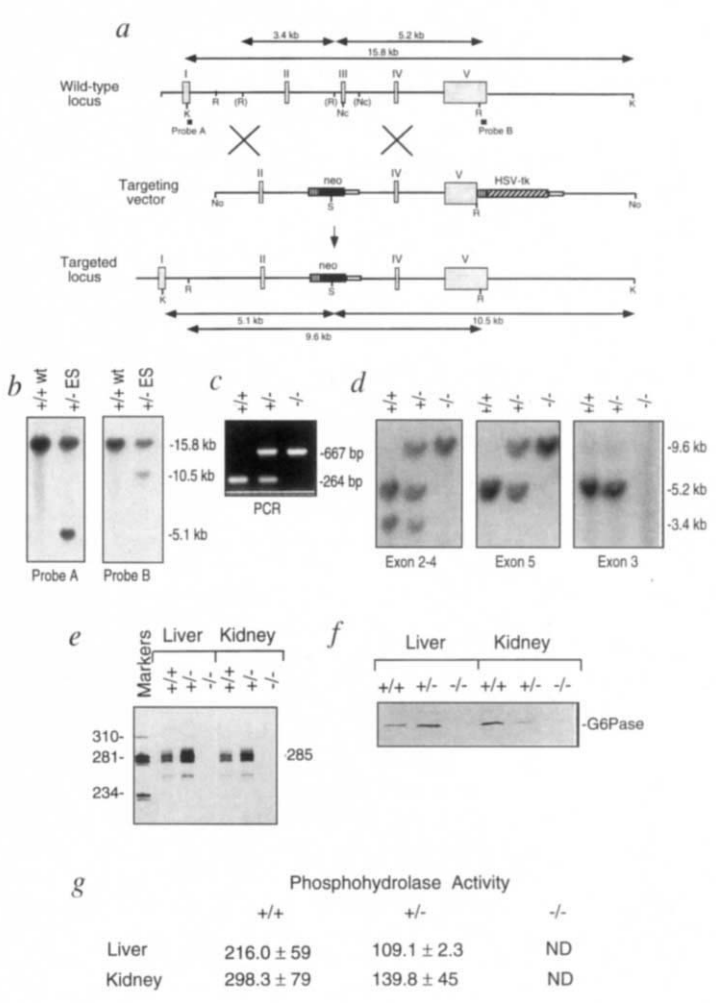

Fig. 1 *a*, Targeted-disruption of the murine *G6Pase* gene. The wild-type locus is presented along with the targeting vector and the anticipated outcome of the recombination (targeted locus). Introns are denoted as lines, exons as boxes. The PGK-1 promoters driving the *neo* and *HSV-tk* genes are denoted as hatched boxes. Gene targeting results in the replacement of exon 3 and the associated introns with a neo cassette that contains a diagnostic *Sfu*I site. (K, *Kpn*I; R, *Eco*RI; Nc, *Nco*I; No, *Not*I; S, *Sfu*I.) *b*, Southern blot analysis of genomic DNA from wild-type (wt, +/+) and targeted ES (+/–) clones digested with *Kpn*I and *Sfu*I. Probes A and B, which are denoted by solid boxes in (*a*), were used to distinguish the recombinant and wild-type clones. The endogenous wild-type (+/+) locus yielded the expected 15.8-kb *Kpn*I band with either probe A or B. The targeted ES (+/–) locus yielded the expected 15.8-kb *Kpn*I and 5.1-kb *Kpn*I/*Sfu*I bands with probe A, and the expected 15.8-kb *Kpn*I and 10.5-kb *Sfu*I/*Kpn*I bands with probe B, confirming the correct targeting event. *c*, PCR analysis of genomic DNA from tail biopsies of F1 intercross progeny. To distinguish between wild-type (+/+), heterozygous (+/–), and homozygous (–/–) animals, an exon 3-specific primer pair, E3/I3, was used to amplify a 264-bp fragment in the wild-type (+/+) and heterozygous (+/–) animal, and a neo-specific primer pair, neo1/neo2, was used to amplify a 667-bp fragment of the introduced *neo* gene of the heterozygous and homozygous (–/–) animals. *d*, Southern blot analyses of *Eco*RI digested genomic DNA from tail biopsies of F1 intercross progeny. Exons 2 to 4, exon 5, and exon 3 specific probes were used to identify the genotype of the F2 mice. The expected sizes of the digested fragments hybridized with the probes are shown in (*a*). As predicted, the G6Pase$^{+/+}$ mice yielded 5.2- and 3.4-kb bands with an exon 2 to 4 specific probe and a 5.2-kb band with an exon 5 or exon 3 specific probe. The G6Pase$^{+/-}$ mice yielded 9.6-, 5.2-, and 3.4-kb bands with an exon 2 to 4 specific probe, 9.6- and 5.2-kb bands with an exon 5 specific probe, and a 5.2-kb band with an exon 3 specific probe. The G6Pase$^{-/-}$ mice yielded a 9.6-kb band with both exon 2 to 4 and exon 5 specific probes but did not hybridize with an exon 3 specific probe. Restriction sites in parentheses were destroyed after the targeting event. *e–g*, Lack of *G6Pase* mRNA, protein, or enzyme activity, respectively, in G6Pase$^{-/-}$ mice. Data were obtained from G6Pase$^{-/-}$ mice and their age-matched G6Pase$^{+/+}$ and G6Pase$^{+/-}$ littermates at 20 to 21 days of age. *e*, Ribonuclease protection analysis of total liver (20 µg) or kidney (10 µg) RNA using an uniformly labelled antisense riboprobe which corresponds to nucleotides 356 to 640 of the murine *G6Pase* cDNA encompassing exons 2 to 4. The *Hin*fI digest of ΦX174 was used as markers. *f*, Western blot analysis of liver and kidney lysates (20 µg) using a rabbit antiserum against the carboxyl terminus of murine G6Pase. *g*, Microsomal G6P phosphohydrolase activity. Liver and kidney microsomes were prepared from 20-day-old G6Pase$^{+/+}$, G6Pase$^{+/-}$, or G6Pase$^{-/-}$ mice from the same litter. The activity is expressed as nmol/min per mg protein and data are presented as mean ± SEM. ND, nondetectable.

© 1996 Nature Publishing Group http://www.nature.com/naturegenetics

tion[2], and we observed no *in utero* lethality. Genotyping of 197 F2 mice also indicated that the targeted mutation is transmitted in a classical mendelian fashion. However, the G6Pase$^{-/-}$ mice weighed significantly less than the G6Pase$^{+/+}$ or G6Pase$^{+/-}$ mice throughout their postnatal development (Fig. 2*a*), implying that the homozygous mutant mice had slower growth rates compared to their G6Pase$^{+/+}$ or G6Pase$^{+/-}$ littermates. A reduced growth rate is also observed in human GSD-1a patients[2,3].

An initial clinical presentation in human GSD-1a cases is hypoglycaemic seizure[2,3]. The mutant mice showed similar trends. The mean plasma glucose level in homozygous mutant mice (0.20 g/l) was significantly lower than those in wild-type (1.38 g/l) or heterozygous (1.31 g/l) littermates (Fig. 2*b*). Furthermore, some of the G6Pase$^{-/-}$ mice suffered seizures that could be relieved by glucose injection. Human GSD-1a patients also present with hyperlipidaemia, hyperuricaemia, and lactic acidaemia[2,3]. Similarly, the G6Pase$^{-/-}$ mice showed an 8-fold elevation of plasma triglyceride (Fig. 2*c*), a 6-fold elevation of plasma cholesterol (Fig. 2*d*), and a 3-fold elevation of plasma uric acid (Fig. 2*e*) compared to the G6Pase$^{+/+}$ and G6Pase$^{+/-}$ animals. In contrast to human GSD-1a patients, however, plasma lactate concentrations were not elevated in the G6Pase$^{-/-}$ mice (Fig. 2*f*).

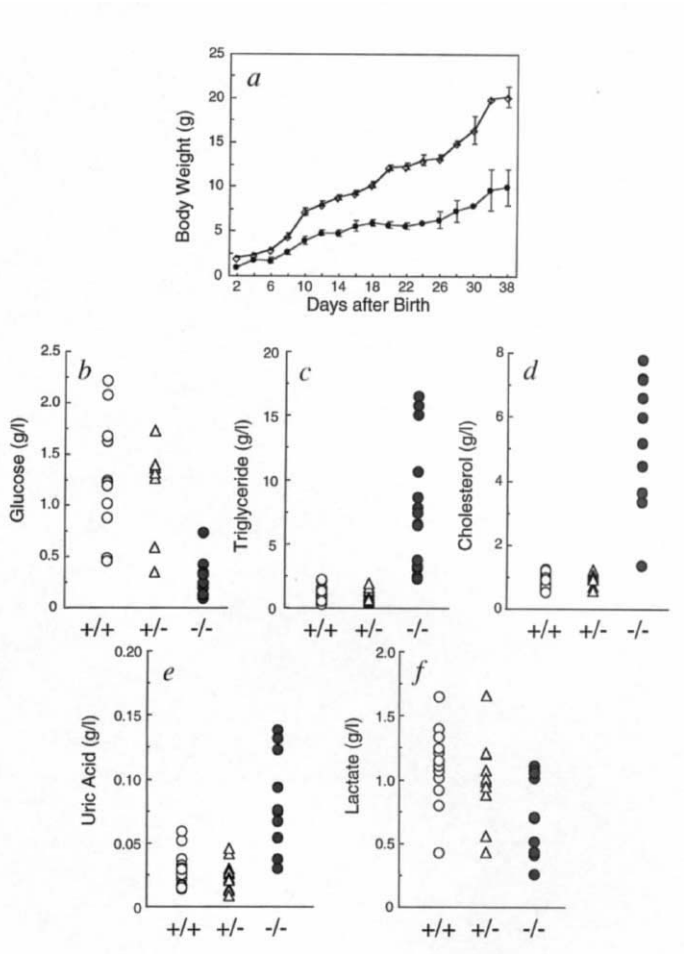

Fig. 2 *a*, Postnatal development of G6Pase$^{+/+}$, G6Pase$^{+/-}$, and G6Pase$^{-/-}$ mice. Each point represents a minimum of 3 animals and data are presented as mean ± SEM. ◊ = G6Pase$^{+/+}$ and G6Pase$^{+/-}$ mice; ● = G6Pase$^{-/-}$ mice. *b–f*, Plasma glucose (*b*), triglyceride (*c*), cholesterol (*d*), uric acid (*e*) and lactate (*f*) levels. Data were obtained from age-matched littermates at 20 to 21 days of age. The mean values of glucose, triglyceride, cholesterol, uric acid and lactate in G6Pase$^{+/+}$, G6Pase$^{+/-}$ and G6Pase$^{-/-}$ mice are: 1.38, 1.31 and 0.20 g/l (glucose); 0.95, 0.90 and 7.81 g/l (triglyceride); 0.86, 0.94 and 5.47 g/l (cholesterol); 0.026, 0.023 and 0.077 g/l (uric acid); and 0.121, 0.108 and 0.078 g/l (lactate), respectively.

The major internal organs of newborn to 87-day-old G6Pase$^{-/-}$, G6Pase$^{+/+}$, and G6Pase$^{+/-}$ mice were examined. Newborn G6Pase$^{-/-}$ mice showed no histological abnormality in any of the organs examined, except for a mild glycogen accumulation in the liver and renal tubules (data not shown) as evaluated by the periodic acid-Schiff stain[20]. By 5 days of age, however, hepatomegaly and kidney enlargement were evident in the G6Pase$^{-/-}$ mice. Haematoxylin and eosin staining revealed that the G6Pase$^{-/-}$ mice had marked glycogen storage in the hepatocytes of the liver (compare Fig. 3*a* and *b*) which created a uniform mosaic architecture with compression of the sinusoids (Fig. 3*b*), similar to that seen in human GSD-1a patients[21]. There was also marked glycogen accumulation in the tubular epithelial cells of the kidney (compare Fig. 3*d* and *e*), which resulted in their enlargement and compression of the glomeruli (Fig. 3*e*). These results were confirmed by electron microscopy analysis, which also revealed prominent lipid vacuoles in G6Pase$^{-/-}$ hepatocytes (Fig. 3*i*). The severity of glycogen deposition was age-related and was markedly pronounced by 20 to 26 days of age.

While the wet weight of the liver from 18- to 20-day-old G6Pase$^{+/+}$ or G6Pase$^{+/-}$ mice was 3.9 ± 0.18% of body mass, that of age-matched G6Pase$^{-/-}$ mice was 20.7 ± 0.33%. Similarly, the wet weight of both kidneys from G6Pase$^{-/-}$ mutant mice increased to 5.1 ± 0.4% of body mass, compared to 1.7 ± 0.3% in the age-matched G6Pase$^{+/+}$ or G6Pase$^{+/-}$ animals. Brain, heart, lung, thymus, lymph nodes, salivary glands, small intestine, colon, stomach, testis, prostate, seminal vesicles, bone marrow, and spleen showed no obvious histological abnormalities, a result consistent with the human disease.

The G6Pase$^{-/-}$ mice also had dysplasia of the cartilage at 5 days of age; the lesions occurred at the knee joint and epiphyseal plate of the long bones. By 16 days of age, cartilage grew in irregular plates with gross deformity of the joints (compare Fig. 3*g* and *h*).

The majority of G6Pase-deficient mice survived weaning, but less than 12% survived beyond 5 weeks of age. Necropsy analysis of one 87-day-old G6Pase$^{-/-}$ mouse revealed pulmonary edema, severe hepatic lipidosis, and glycogen storage in the liver and kidneys.

© 1996 Nature Publishing Group http://www.nature.com/naturegenetics

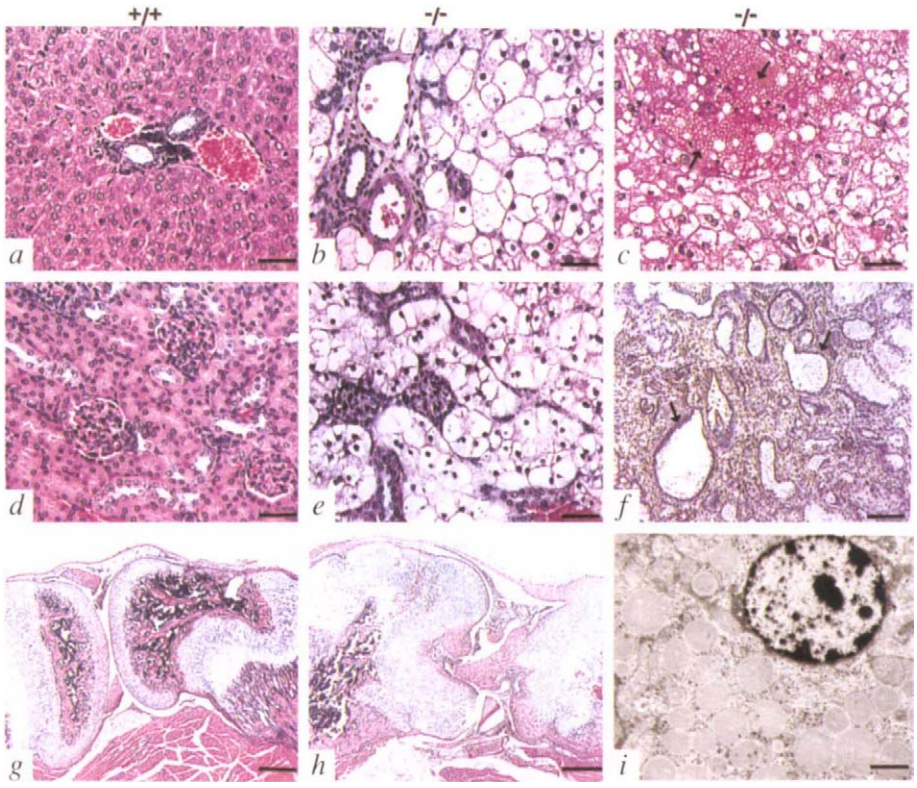

Fig. 3 Histological analyses of liver, kidney and bone from G6Pase$^{+/+}$ and G6Pase$^{-/-}$ mice. *a, b, d, e,* Haematoxylin-eosin stained liver and kidney from G6Pase$^{+/+}$ (*a, d*) and G6Pase$^{-/-}$ (*b, e*) littermates killed at 21 days of age (scale bar, 33.3 μm). The liver shows a diffuse mosaic pattern consistent with marked glycogen accumulation in hepatocytes. The enlargement of kidney tubular epithelial cells, indicative of glycogen deposition resulted in compression of the glomeruli. *c, f,* Necropsy analysis of liver (*c,* scale bar, 33.3 μm) and kidney (*f,* scale bar, 133 μm) of one 87-day-old G6Pase$^{-/-}$ mouse. The liver showed marked necrosis with blood lakes (indicated by arrows), and the kidney showed tubular dilatation (indicated by arrows), atrophic glomeruli, and interstitial fibrosis. *g, h,* Haematoxylin-eosin stained knee joints from G6Pase$^{+/+}$ (*g*) and G6Pase$^{-/-}$ (*h*) littermates killed at 16 days of age (scale bar, 333 μm). The G6Pase$^{-/-}$ mice showed gross deformity of the joint with cartilage growing in irregular plates. *i,* An electron micrograph of liver from a G6Pase$^{-/-}$ mouse killed at 26 days of age. Note the abundance of glycogen particles and lipid droplets in the cytoplasm (scale bar, 6.67 μm).

The liver (Fig. 3*c*) showed marked necrosis with blood lakes. The kidneys (Fig. 3*f*) showed atrophic glomeruli, mild interstitial fibrosis, tubular dilatation, and atrophy. The lesions in both organs were life-threatening.

Role of G6Pase in G6P transport

This well defined mouse model of GSD-1a provides an opportunity to examine the two theories proposed for G6Pase catalysis. The multi-functional conformation-substrate-transport model[5] is supported by observations that G6P transport and hydrolysis appear synchronous[6]. The multi-component translocase-catalytic unit model[7,8], however, is supported by observations that liver microsomes in GSD-1b and 1c patients have G6Pase activity but no substrate or product transport activity[9–12]. To assess these two models, we examined microsomal G6P transport and hydrolysis (Fig. 4*a–d*). Both the liver and kidney microsomes from G6Pase$^{+/+}$ mice transported G6P efficiently, reaching a steady-state level within 3 min (Fig. 4*a, b*). In contrast, there was no significant G6P uptake by the liver or kidney microsomes of the G6Pase$^{-/-}$ littermates (Fig. 4*a, b*), implying that either G6Pase activity is required for G6P transport into the microsomes, or that G6Pase is its own substrate transporter. To elucidate this aspect, the effect of vanadate, a potent competitive inhibitor of G6Pase[22] was examined. If transport and catalysis are performed by a single site in one protein, both activities should show the same sensitivity to a competitive inhibitor. If different proteins or sites are involved, different sensitivities are expected. Hydrolysis by G6Pase was measured in disrupted microsomes, independent of uptake, under saturating conditions (10 mM G6P) and conditions optimal for the uptake assay (0.2 mM G6P). In the liver, G6P uptake was inhibited 70% by 50 μM vanadate while G6P hydrolysis, under similar conditions, was much less sensitive requiring 1.1 mM vanadate for 70% inhibition (Fig. 4*c*). However, vanadate did not abolish G6P uptake completely as low levels of transport were observed even in the presence of 4 mM vanadate. On the other hand, G6P hydrolysis was completely inhibited by 2 mM vanadate (Fig. 4*c*). Similar differential sensitivities were noted in the kidney (Fig. 4*d*).

While the vanadate study demonstrated that G6P transport and hydrolysis are not performed by a single site of one protein, it could not distinguish between one protein with two functionally distinct domains or two different proteins. To help distinguish between these, we examined the role of liver and kidney in G6Pase catalysis. Although both liver and kidney microsomes from G6Pase$^{+/+}$ mice transported G6P efficiently (Fig. 4*a, b*), G6P uptake by whole kidney microsomes (0.22 nmol/mg) was only 25% of the rate

© 1996 Nature Publishing Group http://www.nature.com/naturegenetics

of liver microsomes (0.88 nmol/mg). When the tissues were sectioned and stained for G6Pase activity, the entire liver stained positive (Fig. 4*e*) while in the kidney only the cortex tubules, which represent about 25% of the kidney mass, stained positive (Fig. 4*f*). Therefore, taking the distribution of cells with G6Pase into account, uptake of G6P, on a per cell mass basis, is similar between liver and kidney (approximately 0.88 nmol/cell mass). However, on a per cell mass basis, assuming that G6Pase-containing cells in the kidney represent 25% of the kidney mass, the catalytic activities are markedly different (liver: kidney = 216: 1193 nmol/min per cell mass) between the two organs (Fig. 1*g*). Hence, G6P transport requires, but is not performed by, G6Pase.

Discussion

We have generated an animal model of GSD-1a by gene targeting and have shown that the G6Pase$^{-/-}$ mice manifest essentially the same pathophysiology as human GSD-1a patients, including hypoglycaemia, growth retardation, hepatomegaly, kidney enlargement, hyperlipidaemia, and hyperuricaemia. Human GSD-1a patients who do not receive dietary treatment die early, usually in the teens, of liver and/or kidney complications. Histopathological examinations of the G6Pase$^{-/-}$ animals revealed marked glycogen storage in the liver and kidney, and fat deposition in hepatocytes. The G6Pase$^{-/-}$ mice survived an average of 4 to 5 weeks and necropsy analysis revealed evidence of severe liver and renal lesions. The extensive similarities between homozygous mutant animals and human GSD-1a patients indicate that the G6Pase$^{-/-}$ mouse is a valid animal model for the study of GSD-1a.

While we found extensive phenotypic similarities between GSD-1a patients and our G6Pase$^{-/-}$ mice, we also noted some differences. The blood lactate levels are usually elevated in GSD-1a patients[2,3], but no increase in serum lactate was observed in G6Pase$^{-/-}$ mice. At present, we do not know the reasons for this discrepancy. It is possible that lactate, produced by glycolysis, is more rapidly taken up by the mouse liver for fatty acid synthesis. We also observed that G6Pase$^{-/-}$ pups, as young as 5 days of age, displayed cartilage dysplasia at both the knee joints and the epiphyseal plate of the long bones. To our knowledge, such an abnormality has not been reported as one of the early manifestations of human GSD-1a. While cartilage dysplasia may be unique to rodents, the bone lesions could also be a previously unrecognized feature of human GSD-1a. In this context, it should be noted that while many clinical manifestations of GSD-1a had been documented over the last four decades, it was only in 1988 that the kidney involvement and its subsequent serious implications in the disease were reported[23]. Thus, cartilage dysplasia in human GSD-1a patients may warrant further assessment.

Our mouse model of GSD-1a has provided an opportunity to examine the two theories of G6Pase catalysis. The conformation-substrate transport model[5,6] proposes that G6Pase has both the catalytic activity and the role of transport of G6P across the microsome membranes. The translocase-catalytic unit model[7–12] proposes that there are separate G6Pase catalytic and G6P transport proteins. Both models have to explain the heterogeneity of GSD-1, particularly the

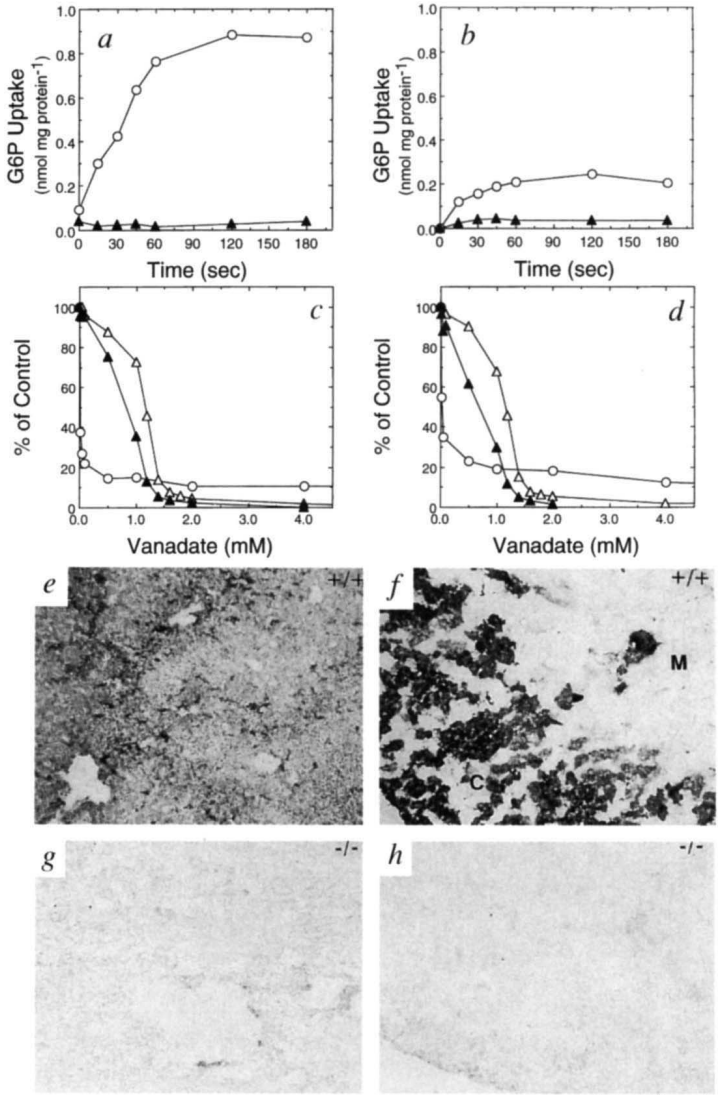

Fig. 4 *a, b,* Uptake of [U-^{14}C]G6P into liver (*a*) and kidney (*b*) microsomes of G6Pase$^{+/+}$ (○) and G6Pase$^{-/-}$ (▲) mice. *c, d,* Effects of vanadate on G6Pase$^{+/+}$ mouse liver (*c*) and kidney (*d*) microsomal [U-^{14}C]G6P uptake (○) and G6P hydrolysis (△, ▲) in the presence of 10 mM (△) or 0.2 mM (○, ▲) G6P. *e–h,* Histochemical analysis of G6Pase activity in liver (*e, g*) and kidney (*f, h*) of G6Pase$^{+/+}$ (*e, f*) and G6Pase$^{-/-}$ (*g, h*) mice. Fresh tissue specimens were sectioned and G6Pase activity was analysed using the method of lead trapping of phosphate generated by G6P hydrolysis. C = cortex; M = medulla.

© 1996 Nature Publishing Group http://www.nature.com/naturegenetics

difference between GSD-1a, in which the patients' microsomes lack G6Pase activity; and GSD-1b, in which the intact microsomes lack G6Pase activity, but disrupted microsomes have G6Pase activity (a G6P transport problem[8–10]).

Our finding that the knockout of the *G6Pase* gene destroys both G6Pase activity and G6P transport provides direct evidence of the tight coupling between G6P transport and G6Pase activity which had previously been inferred from kinetic studies of G6Pase catalysis[6]. While this finding is consistent with the conformation-substrate transport model, it is not inconsistent with the translocase-catalytic unit model. In previous work[16] we have been unable to detect mutations in the *G6Pase* gene of GSD-1b patients, a finding that supports the translocase-catalytic unit model. Further support for this model is provided by the current comparison of G6Pase catalysis in liver and kidney. On a per cell mass basis, uptake of G6P is similar between liver and kidney, but the catalytic activities are markedly different between the two organs. This finding has two implications. First, it excludes the possibility that the linkage between G6P transport and hydrolytic activities is a consequence of the catalytic activity reducing the concentration of G6P in the ER, thus allowing the transporter to function more efficiently. Second, it argues strongly that there must be two proteins, one for G6P transport and one for catalysis, with transport the rate limiting step. We therefore propose a modified translocase-catalytic unit model, in which G6Pase catalysis consists of two tightly coupled reactions, G6P transport and G6P hydrolysis. Inactivation of transport prevents substrate access to the hydrolytic center while inactivation of hydrolysis abolishes transport by uncoupling an essential link.

While the liver has been considered the predominant site of gluconeogenesis, the role of kidney G6Pase in human glucose homeostasis has been unclear. Efforts to correct the G6Pase deficiency in GSD-1a patients have focused on both renal and liver allografts. While renal transplants have failed to maintain normoglycaemia in GSD-1a patients[24,25], liver transplants have appeared to correct hypoglycaemia and several other biochemical abnormalities associated with GSD-1a[26,27]. This is consistent with our findings. While whole kidney microsomes contain a higher specific activity than liver microsomes (Fig. 1*g*), the rate-limiting uptake, the tight coupling of G6P transport-hydrolysis, and the smaller tissue mass of the G6Pase-containing cells in the kidney, would combine to diminish the role of the kidney in glucose homeostasis. In comparison, the larger tissue mass of the liver hepatocytes, all of which express G6Pase, is consistent with the greater success of the liver transplants.

We are now pursuing this *G6Pase*-deficient mouse model to develop novel therapeutic approaches for GSD-1a, to increase our understanding of the biology and pathophysiology of this disorder, and for further analysis of the mode of G6Pase catalysis.

Methods

Construction of targeting vector. The targeting vector was constructed by ligating the *Nco*I–*Eco*RI fragment containing exon 4 and part of exon 5 of the murine *G6Pase* gene into the *Eco*RI site of the *Eco*RI/*Bam*HI-fragment of the pPNT plasmid[17]. This plasmid was circularized, re-linearized with *Xho*1, blunt-ended, and ligated with the polished *Eco*RI-fragment containing exon 2 of the murine *G6Pase* gene. The construct was verified by restriction endonuclease mapping and DNA sequencing.

Transfection of ES cells. The targeting-construct, linearized at the *Not*I site, was introduced into J1 ES cells by electroporation and the cells were subjected to selection with G418 (400 μg/ml) and gancyclovir (2 μM)[19]. The cell lines were then screened by Southern blotting for disruption of the *G6Pase* gene using two probes corresponding to specific 5' (nucleotides 22–300 in exon 1) or 3' (nucleotides 1804–2091 in exon 5) regions of the murine *G6Pase* gene.

Generation of *G6Pase*-deficient mice. Chimaeric mice were generated by injection of the *G6Pase*-disrupted ES cells into C57BL/6 blastocysts which were then implanted into the uterine horn of pseudopregnant FVB/N foster mice. Two independently targeted ES cell lines, E60 and E71, were used to generate two lines of mice carrying the *G6Pase* null mutation to ensure that the anticipated *G6Pase* null phenotype would result from a disruption of the *G6Pase* gene versus nonhomologous recombination. The chimaeric mice were mated with C57BL/6 or CD1 mice and germline transmission of the *G6Pase* null allele in F1 heterozygous mice was examined by PCR and Southern analysis of DNA extracted from the tails. Heterozygous animals were interbred to generate homozygous mice lacking the functional *G6Pase* gene.

An exon 3 specific primer pair, E3 (5'–AAGTCCCTCTGGCCATGCCATGGG–3', nucleotides 424–447 in exon 3) and I3 (5'–CCAAGCATCCTGTGATGCTAACTC–3', within intron 3) and a *neo*-specific primer pair, neo1 (5'–ATACGCTTGATCCGGCTACCTGCC–3') and neo2 (5'–CATTTGCAC TGCCGGTAGAACTCC–3'), were used to identify the genotype of the F2 mice by PCR. The neo1/neo2 primers are expected to amplify a fragment of 667 bp in the *neo* gene of the targeted *G6Pase* null locus and the E3/I3 primers are expected to amplify a fragment of 264 bp in the wild-type *G6Pase* locus. Southern blot analysis of tail genomic DNA digested with *Eco*RI was used to confirm the genotype of the F2 mice. Exon 2 to 4, and exon 5 specific probes contained nucleotides 306–633 and 669–1145 of the murine *G6Pase* cDNA[13], respectively. The exon 3 specific probe (428 bp) encompassing exon 3 and the associated intron 3 was obtained by PCR amplification of the murine *G6Pase* gene using E3 and an intron 3 primer (5'–GAGGTGACTCCAGGATGA–3').

Ribonuclease protection and western blot analysis. Ribonuclease protection analysis of liver and kidney RNA was performed using an antisense riboprobe spanning nucleotides 356–640 of the murine *G6Pase* cDNA[13], which encompasses 68 bp of exon 2, the entire exon 3, and 111 bp of exon 4. Western blot analysis of liver and kidney microsomal G6Pase was performed using a rabbit antiserum against the carboxyl terminus of mouse G6Pase (amino acids 247 to 357). This carboxyl terminus was produced by subcloning nucleotides 821–1153 of the murine *G6Pase* into a bacterial expression vector pGEX-4T-1 and produced as a glutathione-S-transferase fusion protein (Pharmacia, NJ).

Phosphohydrolase assay. Microsomal preparations and phosphohydrolase assays were performed as described[28]. The phosphohydrolase assays detect accurately 1 nmol of phosphate produced by hydrolysis of G6P. Disrupted microsomal membranes were prepared by incubating intact membranes in 0.2% deoxycholate for 20 min at 0 °C. Non-specific phosphatase activity in microsomes was estimated by preincubating microsomal preparations at pH 5 for 10 min at 37 °C, a condition that inactivates the thermal labile G6Pase[29]. Enzyme histo-

© 1996 Nature Publishing Group http://www.nature.com/naturegenetics

chemistry of G6Pase[30] was carried out by incubating fresh liver or kidney sections (10 μm) for 10 min, at room temperature, in a solution containing 40 mM Tris-maleate, pH 6.5, 10 mM G6P, 300 mM sucrose, and 3.6 mM lead nitrate. The trapped lead phosphate was visualized following conversion to the colored lead sulfide. Glucose-1-P, which is not a substrate for G6Pase, was used as a negative control.

Phenotype analysis. Mice were maintained on a normal diet without any restriction on dietary intake. To prevent feeding competition while suckling, litter sizes were decreased by removing some of the G6Pase$^{+/+}$ and G6Pase$^{+/-}$ littermates. Plasma samples were collected by orbital bleeding using a heparinized pasteur pipet (Baxter Healthcare Co.), transferred to a fluoride-oxalate-treated capillary blood collecting tube (Terumo Medical Co., Elkton, MD), and allowed to settle on ice. Glucose, triglycerides, total cholesterol, uric acid, and lactate in plasma samples were analysed using kits obtained from Sigma Diagnostics.

For haematoxylin-eosin staining, tissues were preserved in 10% neutral buffered formalin and sectioned at 4–6 μm. For electron microscope analysis, tissues from G6Pase$^{-/-}$ mice were fixed in 2.5% glutaldehyde, postfixed in osmium tetroxide and embedded in epoxy resin. Thin sections were stained with uranyl acetate and lead citrate.

G6P uptake analysis. G6P uptake was determined by incubating microsomes (40 μg) in a reaction mixture (100 μl) containing 50 mM Tris-HCl, pH 7.3, 250 mM sucrose, 2 mM EGTA, 0.2 mM G6P, and 1 μCi [U-^{14}C]G6P. The reaction was stopped at the appropriate time by the addition of 50 volumes of 50 mM Tris-HCl, pH 7.5, 250 mM sucrose, 25 mM KCl, 5 mM $MgCl_2$, and 8 mM $CaCl_2$, and filtered immediately through a nitrocellulose filter (BA85, Schleicher & Schuell) essentially as described[6], except a single well filtration apparatus was used. Microsomal preparations from 5 to 16 day-old G6Pase$^{+/+}$ and G6Pase$^{-/-}$ mice were used. The age of the animals had little effect on microsomal G6P uptake. Moreover, glycogen did not interfere with uptake since removal of glycogen had little effect on the uptake measurement.

Acknowledgements

We thank A. Mukherjee, I. Owens and M. Chamberlin for critical reading of the manuscript; K. Nagashina, V. Marchall and J. Watson for technical support; J.-F. St-Denis for advice on transport studies; and Syntex Research for their gift of gancyclovir.

Received 16 January; accepted 1 April 1996.

1. Nordlie, R.C. & Sukalski, K.A. Multifunctional glucose-6-phosphatase: a critical review, in *The Enzymes of Biological Membranes* (ed Martonosi, A.N.) 349–398 (Plenum Press, New York, 1985).
2. Chen, Y.-T. & Burchell, A. Glycogen storage diseases. in *The Metabolic Basis of Inherited Diseases* 7th edn. (eds Scriver, C.R., Beaudet, A.L., Sly, W.S. & Valle, D.) 935–965 (McGraw-Hill Inc., New York, 1994).
3. Moses, S.W. Pathophysiology and dietary treatment of the glycogen storage diseases. *J. Pediat. Gastroenterol. Nutr.* **11**, 156–174 (1990).
4. Waddell I.D. & Burchell, A. Transverse topology of glucose-6-phosphatase in rat hepatic endoplasmic reticulum. *Biochem J.* **275**, 133–137 (1991).
5. Schulze, H.U., Nolte, B. & Kannler. R. Evidence for changes in the conformational status of rat liver microsomal glucose-6-phosphate: phosphohydrolase during detergent-dependent membrane modification. *J. Biol. Chem.* **261**, 16571–16578 (1986).
6. St-Denis, J.-F., Berteloot, A., Vidal, H., Annabi, B. & van de Werve, G. Glucose transport and glucose-6-phosphate hydrolysis in intact rat liver microsomes. *J. Biol. Chem.* **270**, 21092–21097 (1995).
7. Arion, W.J., Lange, A.J., Walls, H.E. & Ballas, L.M. Evidence of the participation of independent translocases for phosphate and glucose-6-phosphate in the microsomal glucose-6-phosphatase system. *J. Biol. Chem.* **255**, 10396–10406 (1980).
8. Burchell, A. Molecular pathology of glucose-6-phosphatase. *FASEB J.* **4**, 2978–2988 (1990)
9. Lange, A.J., Arion, W.J. & Beaudet, A.L. Type 1b glycogen storage disease is caused by a defect in the glucose-6-phosphate translocase of the microsomal glucose-6-phosphatase system. *J. Biol. Chem.* **255**, 8381–8384 (1980).
10. Igarashi, Y., Kato, S., Narisawa, K. & Tada, K. A direct evidence for defect in glucose-6-phosphatase transport system in hepatic microsomal membrane of glycogen storage disease type 1b. *Biochem. Biophys. Res. Commun.* **119**, 593–597 (1984).
11. Nordlie, R.C., Sukalski, K.A., Munoz, J.M. & Baldwin, J.J. Type 1c, a novel glycogenosis. *J. Biol. Chem.* **258**, 9739–9744 (1983).
12. Waddell, I.D., Hume, R. & Burchell, A. A direct method for the diagnosis of human hepatic type 1b and type 1c glycogen-storage disease. *Clin. Sci.* **76**, 573–579 (1989).
13. Shelly, L.L. *et al.* Isolation of the gene for glucose-6-phosphatase, the enzyme deficient in glycogen storage disease type 1a. *J. Biol. Chem.* **268**, 21482–21485 (1993).
14. Lei, K.-J., Shelly, L.L., Pan, C.-J., Sidbury, J.B. & Chou, J.Y. Mutations in the glucose-6-phosphatase gene that cause glycogen storage disease type 1a. *Science* **262**, 580–583 (1993).
15. Lei, K.-J. *et al.* Genetic basis of glycogen storage disease type 1a: prevalent mutations at the glucose-6-phosphatase locus. *Am. J. Hum. Genet.* **57**, 766–771 (1995).
16. Lei, K.-J. *et al.* Mutations in the glucose-6-phosphatase gene are associated with glycogen storage disease type 1a and 1aSP but not 1b and 1c. *J. Clin. Invest.* 95, 234–240 (1995).
17. Tybulewicz, V.L.J., Crawford, C.E., Jackson, P.K., Bronson, R.T. & Mulligan, R.C. Neonatal lethality and lymphopenia in mice with a homozygous disruption of the c-abl proto-oncogene. *Cell* **65**, 1153–1163 (1991).
18. Love, P.E. *et al.* T cell development in mice that lack the ς chain of the T cell antigen receptor complex. *Science* **261**, 918–921 (1993).
19. Mansour, S.L., Thomas, K.R. & Capecchi, M.R. Disruption of the proto-oncogene int-2 in mouse embryo-derived stem cells: a general strategy for targeting mutations to non-selectable genes. *Nature* **336**, 348–352 (1988).
20. Chayen, J. & Bitensky, L. Analysis of chemical components of cells and tissues. in *Practical Histochemistry*. 45–134 (John Wiley & Sons, New York, 1991).
21. McAdams, A.J., Hug, G. & Bove, K.E. Glycogen storage disease types I to X: Criteria for morphologic diagnosis. *Hum. Pathol.* **5**, 463–487 (1974).
22. Singh, J., Nordlie, R.C. & Jorgenson, R.A. Vanadate: a potent inhibitor of multifuntional glucose-6-phosphatase. *Biochim. Biophys. Acta* **678**, 477–482 (1981).
23. Chen, Y.-T., Coleman, R.A., Scheiman, J.I., Kolbeck, P.C. & Sidbury, J.B. Renal disease in type I glycogen storage disease. *N. Engl. J. Med.* **318**, 7–11 (1988).
24. Emmett, M. & Narins, R.G. Renal transplantation in type 1 glycogenosis: failure to improve glucose metabolism. *JAMA* **239**, 1642–1644 (1978).
25. Chen, Y.-T. & Scheinman, J.I. Hyperglycaemia associated with lactic acidaemia in a renal allograft recipient with type 1 glycogen storage disease. *J. Inher. Metab. Dis.* **14**, 80–86 (1991).
26. Malatack, J.J. *et al.* Liver transplantation for type 1 glycogen storage disease. *Lancet* 1, 1073–1075 (1983).
27. Kirschner, B.S., Baker, A.L. & Thorp. F.K. Growth in adulthood after liver transplantation for glycogen storage disease type 1. *Gastroenterol.* **101**, 238–241 (1991).
28. Burchell, A., Hume, R. & Burchell, B. A new microtechnique for the analysis of the human hepatic microsomal glucose-6-phosphatase system. *Clim. Chim. Acta* **173**, 183–192 (1988).
29. Hers, H. G. in *Advances in Metabolic Disorders*. Vol 1 (eds Levine, R., & Luft, L) 1–44 (Academic Press, London, 1964).
30. Teutsch, H.F. Chemomorphology of liver parenchyma: Qualitative histochemical distribution patterns and quantitative sinusoidal profiles of G6Pase, G6PDH and malic enzyme activity and of glycogen content. in *Progress in Histochemistry and Cytochemistry*. Vol. 14 (Laupp & Gobel, New York, 1981).